Direct Observation of Spin-Torque Driven Magnetization Reversal through Nonuniform Modes

J. P. Strachan,[1,*] V. Chembrolu,[1] Y. Acremann,[2] X. W. Yu,[1] A. A. Tulapurkar,[3] T. Tyliszczak,[4] J. A. Katine,[5] M. J. Carey,[5] M. R. Scheinfein,[6] H. C. Siegmann,[2] and J. Stöhr[3]

[1]*Department of Applied Physics, Stanford University, Stanford, California 94305, USA*
[2]*PULSE Center, Stanford Linear Accelerator Center, Menlo Park, California 94025, USA*
[3]*Stanford Synchrotron Radiation Laboratory, Menlo Park, California 94025, USA*
[4]*Advanced Light Source, LBNL, Berkeley, California 94720, USA*
[5]*Hitachi Global Storage Technologies, San Jose, California 95135, USA*
[6]*Department of Physics, Simon Fraser University, Burnaby BC, Canada U5A 156*
(Received 23 March 2008; published 16 June 2008)

We present time-resolved x-ray images with 30 nm spatial and 70 ps temporal resolution, which reveal details of the spatially resolved magnetization evolution in nanoscale samples of various dimensions during reversible spin-torque switching processes. Our data in conjunction with micromagnetic simulations suggest a simple unified picture of magnetic switching based on the motion of a magnetic vortex. With decreasing size of the magnetic element the path of the vortex core moves from inside to outside of the nanoelement, and the switching process evolves from a curled nonuniform to an increasingly uniform mode.

DOI: 10.1103/PhysRevLett.100.247201 PACS numbers: 75.75.+a, 68.37.Yz, 75.60.Jk, 85.75.−d

The spin-torque effect [1,2] has been verified experimentally by many studies [3–6] and manifests itself in full magnetization reversal [4–7] as well as steady-state precessional modes [8–11] of a nanoscale magnetic element. These capabilities have applications for both magnetic data storage and memory as well as dc controlled microwave oscillators. Therefore, understanding the magnetization dynamics under the influence of spin torque has been a very active area of research. To date, the dominant measurement technique has been magnetoresistance measurements, which measure the average relative alignment between a free and a polarizing layer.

Some of the open issues for spin-torque driven switching include an understanding of the dominant physical processes involved, the intermediate magnetic configurations that are taken, and the appropriateness of a macrospin [12–14] versus a full micromagnetic [15,16] picture. The macrospin model—in which the free layer magnetization is treated at all times as a uniform single domain (SD)—has failed to quantitatively describe switching as well as features of the precessional dynamics [17]. While it may be suspected that this coherent rotation picture does not describe the switching process, there is no clear consensus on an alternative picture, mainly due to a lack of experimental data and techniques that can probe the spatial variation. Meanwhile, simulations have shown a range of behaviors from the semichaotic [15,17] to the formation of wandering vortices that can obstruct the reversal [18].

Our work directly addresses this issue with time-resolved x-ray images of the spatial variation of the magnetization during reversal. Our previous studies [19] first revealed an unexpected reversal mechanism involving the formation and motion of a vortex across the sample. The general applicability of these results was hindered, however, by the stability of an intermediate curled state in the studied devices. Here we study devices of various dimensions that exhibit reversible switching between fully uniform states. We observe two types of switching: a deterministic process driven by the motion of a vortex and a more stochastic process involving the rotation of bent (C) states.

The samples consist of typical current-perpendicular-to-plane spin valve nanopillars. Fabrication details can be found elsewhere [20]. The free layer is 2 nm of $Co_{0.86}Fe_{0.14}$ and a 3.5 nm Cu spacer separates the free layer from the fixed, polarizing layer. This fixed layer consists of a CoFe(1.8)/Ru(0.8)/CoFe(2.0 nm) synthetic antiferromagnet (SAF). The SAF is pinned by exchange bias to an underlying IrMn layer. For microscopy, we study samples that are of a size where the SD is the only stable state as verified by giant magnetoresistance measurements. The sample cross section is elliptical in shape with dimensions varying from 85×135 nm to 110×180 nm.

Resistance measurements for a nominally identical and representative sample from the same fabrication wafer with dimensions 110×180 nm are shown in Fig. 1. Derived from these measurements are a magnetoresistance of $\Delta R \approx 30\ \mathrm{m}\,\Omega$, switching thresholds $I_{\mathrm{AP}\rightarrow P} = 4.8$ mA, $I_{P\rightarrow \mathrm{AP}} = -8.6$ mA, and a coercivity $H_c = 180$ Oe. A stray field of ~60 Oe due to the fixed layer is present. For all samples discussed here only saturated, uniform states of opposite magnetization were stable [21].

Time-resolved pump-probe measurements were performed using fast current-pulse excitations of 4 ns duration and a 100 ps wide leading edge provided by a pulse generator as described in [19].

In Fig. 2, the observed switching process for the 110×180 nm samples is shown. In total, four nominally identical samples of this size were studied—two at a horizontal orientation that allows sensitivity to M_x and two at a

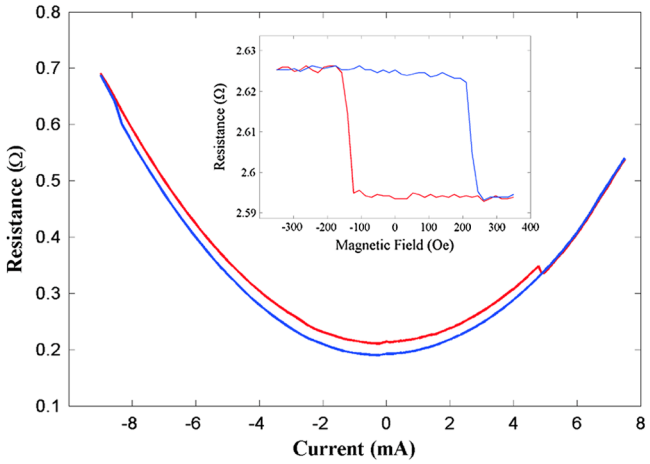

FIG. 1 (color online). Giant magnetoresistance of typical 110 × 180 nm samples, measured with a 100 μA current. Resistance as a function of applied current and (inset) magnetic field.

vertical orientation that is sensitive to M_y. All four samples showed consistent switching behavior. Using two sets of data, one of the M_x component and another of the M_y component, a full vector reconstruction of the magnetization direction at each time point was obtained. Most noticeably the magnetization reversal in Fig. 2 is seen to proceed via highly nonuniform configurations for both current directions. In Fig. 2(a), before the pulse, the magnetization is in a uniform SD state, which is known to be antiparallel to the fixed layer. A 4 ns positive pulse is then applied, which bends the magnetization into a *C*-state configuration [Fig. 2(b)]. A full vortex configuration then follows in Fig. 2(c), and this vortex proceeds across and out of the sample [Figs. 2(d) and 2(e)], leaving behind a switched magnetization. The magnetic configuration remains a reversed *C* state until the current pulse is off and the magnetization relaxes into a SD state in Fig. 2(f). Application of a negative pulse reverses the magnetization [Figs. 2(g)–2(j)] in a similar manner.

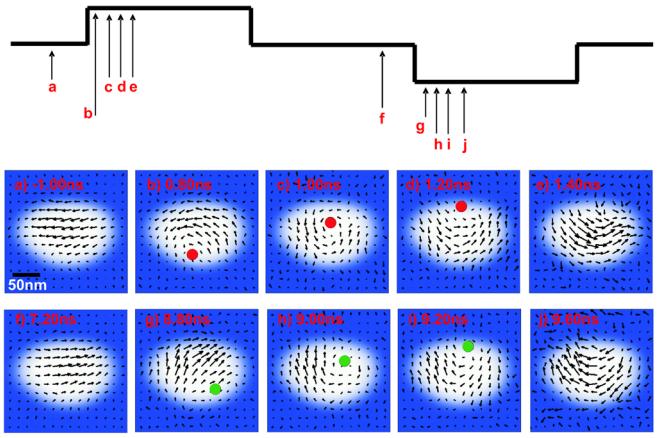

FIG. 2 (color online). Evolution of the magnetization direction during the pulse sequence (shown above) on the 110 × 180 nm sample. The length of the arrows is determined by the x-ray magnetic circular dichroism contrast and the region inside (outside) the pillar is shown by the white (blue) area. A small signal in the nonmagnetic region can be present due to noise and the finite spatial resolution of the measurements. As a guide to the eye, a solid circle (red or green, for right- or left-handed, respectively) labels the estimated position of the vortex core. The uniform antiparallel configuration (a) is switched into a *C* state with a parallel M_x component (b). The switching process involves motion of a magnetic vortex visible in (c). The *C* state relaxes to a uniform state after the falling edge of the pulse (f) and is reversed (g)–(j) by the reset pulse. This reversal also proceeds via highly nonuniform magnetic configurations.

X-ray microscopy measurements were also performed on smaller samples of sizes 85 × 135 nm and 110 × 150 nm. Figure 3 shows the observed switching process for a 110 × 150 nm sample, with similar results seen for the 85 × 135 nm samples. The results show full magnetic reversal for both directions. What is most interesting is the transition regions between the two states. Unlike for the 110 × 180 nm sample, there is no sign of a vortex. The absence of a vortex is also evident from the original orthogonal images used to compose Fig. 3 since a vortex configuration has a distinct appearance in both the vertical and horizontal magnetization components, which was not observed in this case [21].

As seen in Fig. 3(a), before the pulse the magnetization appears uniform within the accuracy of the experiment. During the subsequent two frames [Figs. 3(b) and 3(c)], the arrows indicating magnetic contrast seem to shorten in length. By the next frame [Fig. 3(d)] the magnetization arrows have grown back, but now with a reversed direction. The current pulse has successfully reversed the magnetization, but the details of the switching process are not resolved. The same behavior is seen during the negative pulse.

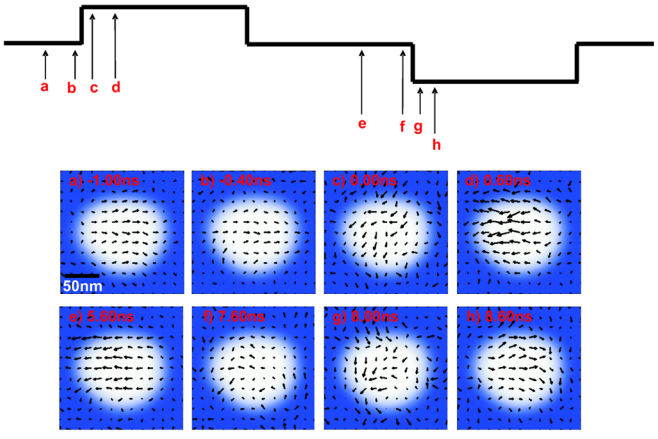

FIG. 3 (color online). Evolution of the magnetization direction during the pulse sequence on the 110 × 150 nm sample measured by way of time-resolved scanning transmission x-ray microscopy.

The reduced in-plane magnetization in Figs. 3(b), 3(c), 3(f), 3(g), and 3(g) is not due to an out-of-plane M_z. This component was zero within the accuracy of our measurement. Since well below T_C the magnetization remains constant, the reduction in the measured magnetization must therefore be an averaging effect arising from the pump-probe technique, which only measures deterministic and repeatable signals. Stochastic processes in which the magnetic configuration varies for different pump-probe switching cycles at the same time delay will lead to a reduction in the measured magnetization at this time delay.

To understand the switching processes in Figs. 2 and 3, micromagnetic simulations were carried out using the "LLG Micromagnetic Simulator" [22] modified to include a spin-torque term [1] resulting from injected polarized current acting on a single layer. Simulations of 85×135 nm and 110×180 nm samples were carried out with a grid size of 3.33 nm, saturation magnetization $M_s = 1.76$ T, damping $\alpha = 0.04$, and spin polarization $\beta = 40\%$. A current step with rise time of 100 ps is driven through the magnetic layer, similar to the actual experiment. The simulation includes the effect of the Oersted field for modeling the dynamics. The observed inhomogeneous switching mechanism shows that the modulation of the current by the magnetization distribution needs to be considered, especially for tunnel magnetoresistance structures with a large magnetoresistance ratio. However, inclusion of an additional spin-torque term due to inhomogeneity in the free layer [23] is difficult to account for and not included in this model.

The results of the simulations are shown in Fig. 4. Beginning with simulations for the 110×180 nm samples, Fig. 4(a) shows a good reproduction of the experimental data of Fig. 2 involving the formation and movement of a vortex across the sample. This vortex-driven switching process was observed for a broad region of the simulation parameter space as one varies the applied charge and spin currents, as well as the damping constant [21]. However, the current threshold needed for complete reversal was found in the simulations to be much higher than that needed in the actual experiments (40 mA rather than 23 mA). The source of this discrepancy is currently uncertain, but may be due to the chosen materials parameters or hidden magnetic edge properties of the actual sample and its interfaces.

The simulations of Fig. 4 allow for a better understanding of the physical mechanism driving the observed reversal process. At the top of Fig. 4(a), the magnetic structure starts in the uniform state antiparallel to the fixed layer and, thus, the initial spin torque on the magnetization is zero. The dominant torque initially is then that of the Oersted field, which is not strong enough to form a full vortex at the experimental currents used (23 mA). The formation of a full vortex by the Oersted field was found to require a current of at least 210 mA. Instead, the magnetization is

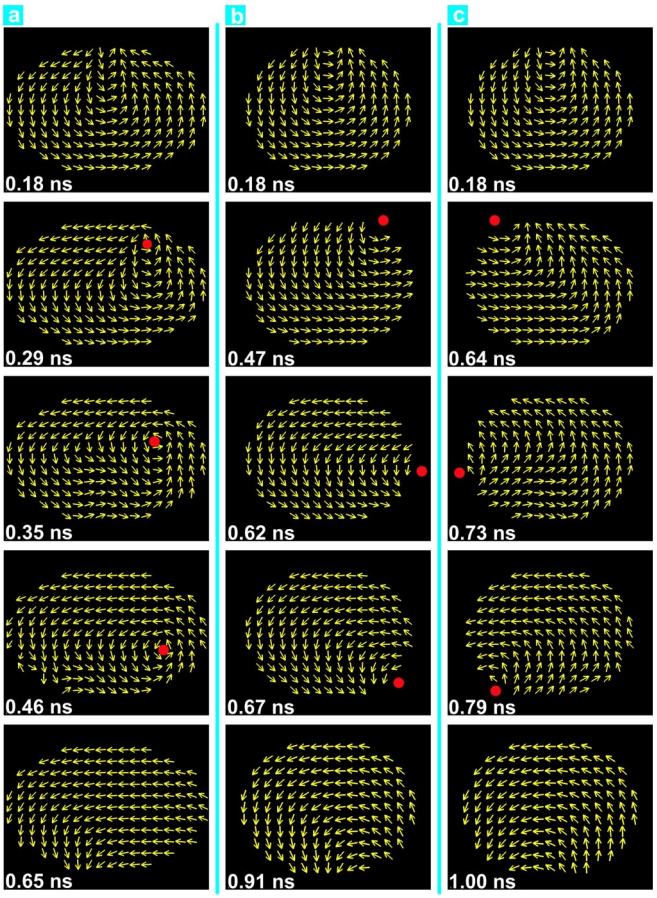

FIG. 4 (color online). Results from simulations. (a) Vortex-driven switching of a 110×180 nm sample. (b) For a 85×135 nm sample, showing instead the flip-over of a C state. In (c) the same simulation is repeated as in (b), but with a 5% reduction in current, leading to a similar reversal but through an alternative path (see text).

bent into a C state [Fig. 4(a), top], which now leads to a nonzero spin torque. Through the action of the spin torque, the C-state nonuniformities are amplified, causing the magnetization at the edges to rotate farther away from the easy axis. This increased bending grows until a vortex is formed near the top of the sample. The vortex is then driven across the sample by the action of the spin torque, which favors growth of the reversed domain. In the final state of the sample, the vortex has been expelled and the magnetization is almost entirely reversed, with a slight C-state bending favored by the Oersted field. The removal of the current and its associated magnetic field allows the sample to relax into a fully uniform state.

The success of the micromagnetics code to reproduce the observed switching behavior of the 110×180 nm sample provides the basis for modeling the experimentally less clear switching behavior for the 110×150 nm and 85×135 nm samples. The results of simulations for the 85×135 nm sample, using the same simulation parameters, are shown in Fig. 4(b). The magnetic element begins

in a uniform state, which then proceeds into a C state. In this case no vortex forms within the sample; however, it is useful to model the C state in a virtual vortex picture, with the vortex core outside of the sample boundary, as illustrated in Fig. 4(b). The C state oscillates clockwise and counterclockwise with growing amplitude until finally tipping over the equator, leading to a reversed C state. In the virtual vortex picture, the horizontal motion of the vortex dominates over the vertical, and the vortex moves around the perimeter of the sample. In contrast, Fig. 4(a) shows a dominance of the vertical motion of the vortex, which proceeds through the sample. We refer to the reversal process as a ''C-state flip-over'' (CSF), and the final state is a switched uniform state with the removal of the current.

The CSF switching can proceed by two paths: the C state can ultimately flip over clockwise, as shown in Fig. 4(b), or counterclockwise, as in Fig. 4(c) (equivalently, the virtual vortex travels down the right or left side). Since either path is allowed, this becomes a bifurcation point for the magnetization dynamics. The simulations exhibit chaotic behavior—a critical dependence on the starting angles of the magnetization and amplitude of the driving current. For the actual experiments at room temperature there are many sources of variation between switching iterations, including current amplitude from pulse to pulse, as well as thermal effects, which lead to magnetization variations across the sample. On the basis of the simulations in Fig. 4 and the data of Fig. 3, we believe it likely that both CSF paths were taken experimentally, and the superposition led to the time-average reduced magnetic signal for the 85×135 nm and 110×150 nm samples. The CSF mechanism can thus explain the switching observed in time-resolved microscopy of these samples.

In summary, we have directly observed two distinct switching processes governing spin-torque driven reversal. One process is the deterministic formation and motion of a vortex through the free magnetic layer [24]. While the Oersted field initiates the nonuniformity, it is through the action of the strong spin torque that the C state is amplified into a vortex state. Slightly smaller samples demonstrated a more chaotic process with no formation of vortices inside the sample. Micromagnetics simulations suggest that now the vortex core simply travels around the periphery of the sample but it may take two paths to finally switch the magnetization.

The x-ray experiments were carried out at the Advanced Light Source (ALS) which like the research program of the Stanford authors is supported by the U.S. Department of Energy, Office of Basic Energy Sciences. Further support came from the Western Institute of Nanoelectronics and sample preparation involved the Stanford Nanofabrication Facility supported by the National Science Foundation under Grant No. ECS-9731293. J. P. S. acknowledges support from the ALS. We would like to thank H. Stoll and B. Van Waeyenberge for providing the detector for the STXM measurements and for fruitful discussions, and Altera, Inc. for providing the development tools through their university program.

*Present address: Information and Quantum Systems Labs, Hewlett-Packard Laboratories, 1501 Page Mill Road, Palo Alto, CA 94304, USA.

[1] J. Slonczewski, J. Magn. Magn. Mater. **159**, L1 (1996).
[2] L. Berger, Phys. Rev. B **54**, 9353 (1996).
[3] M. Tsoi, A. G. M. Jansen, J. Bass, W. C. Chiang, M. Seck, V. Tsoi, and P. Wyder, Phys. Rev. Lett. **80**, 4281 (1998).
[4] J. Sun, J. Magn. Magn. Mater. **202**, 157 (1999).
[5] E. B. Myers, D. Ralph, J. A. Katine, R. N. Louie, and R. A. Buhrman, Science **285**, 867 (1999).
[6] J. A. Katine, F. J. Albert, R. A. Buhrman, E. B. Myers, and D. C. Ralph, Phys. Rev. Lett. **84**, 3149 (2000).
[7] S. Urazhdin, N. O. Birge, W. P. Pratt, and J. Bass, Phys. Rev. Lett. **91**, 146803 (2003).
[8] S. I. Kiselev, J. C. Sankey, I. N. Krivorotov, N. C. Emley, M. Rinkoski, C. Perez, R. A. Buhrman, and D. C. Ralph, Phys. Rev. Lett. **93**, 036601 (2004).
[9] I. N. Krivorotov, N. C. Emley, J. C. Sankey, S. I. Kiselev, D. C. Ralph, and R. A. Buhrman, Science **307**, 228 (2005).
[10] S. Kaka, M. R. Pufall, W. H. Rippard, T. J. Silva, S. E. Russek, and J. A. Katine, Nature (London) **437**, 389 (2005).
[11] W. H. Rippard, M. R. Pufall, S. Kaka, T. J. Silva, S. E. Russek, and J. A. Katine, Phys. Rev. Lett. **95**, 067203 (2005).
[12] Y. B. Bazaliy, B. A. Jones, and S.-C. Zhang, Phys. Rev. B **69**, 094421 (2004).
[13] H. Morise and S. Nakamura, Phys. Rev. B **71**, 014439 (2005).
[14] S. E. Russek, S. Kaka, W. H. Rippard, M. R. Pufall, and T. J. Silva, Phys. Rev. B **71**, 104425 (2005).
[15] J. Miltat, G. Albuquerque, A. Thiaville, and C. Vouille, J. Appl. Phys. **89**, 6982 (2001).
[16] K.-J. Lee, J. Phys. Condens. Matter **19**, 165211 (2007).
[17] K.-J. Lee, A. Deac, O. Redon, J. P. Nozieres, and B. Dieny, Nat. Mater. **3**, 877 (2004).
[18] K.-J. Lee and B. Dieny, Appl. Phys. Lett. **88**, 132506 (2006).
[19] Y. Acremann, J. P. Strachan, V. Chembrolu, S. D. Andrews, T. Tyliszczak, J. A. Katine, M. J. Carey, B. M. Clemens, H. C. Siegmann, and J. Stöhr, Phys. Rev. Lett. **96**, 217202 (2006).
[20] D. Lacour, J. A. Katine, N. Smith, M. J. Carey, and J. R. Childress, Appl. Phys. Lett. **85**, 4681 (2004).
[21] J. P. Strachan, Ph.D. thesis, Stanford University, Department of Applied Physics (2007).
[22] M. R. Scheinfein, LLG Micromagnetic Simulator™, http://llgmicro.home.mindspring.com.
[23] A. Brataas, Y. Tserkovnyak, and G. E. W. Bauer, Phys. Rev. B **73**, 014408 (2006).
[24] The direction of the vortex core may also be switched as observed by B. Van Waeyenberge *et al.*, Nature (London) **444**, 461 (2006).